

Strategic Control of Transverse Jet Shear Layer Instabilities

J. Davitian,* C. Hendrickson,* D. Getsinger,* R. T. M'Closkey,† and A. R. Karagozian‡
University of California, Los Angeles, Los Angeles, California 90095

DOI: 10.2514/1.J050336

This experimental study explores active control of the single gaseous jet in crossflow or transverse jet. Jet nozzles that are flush as well as elevated with respect to the injection wall are considered. These studies develop a strategy for control based on separate experimental findings [Megerian, S., Davitian, J., Alves, L. S. de B., and Karagozian, A. R., "Transverse-Jet Shear-Layer Instabilities. Part 1. Experimental Studies," *Journal of Fluid Mechanics*, Vol. 593, 2007, pp. 93–129], which indicate that the jet's shear layer transitions to global instability when the jet-to-crossflow velocity ratio R lies below a critical range. The R -dependent differences in the stability characteristics suggest the necessity of a two-pronged approach to the controlled excitation of transverse jet penetration and spread, which is explored in this paper. For the transverse jets with relatively large R values, the jet shear layer exhibits convective instability, hence even low-to-moderate-level sinusoidal forcing of the jet can control penetration and spread. For the case where R is relatively low and the shear layer is globally unstable, the self-excited flow can be affected by strong sinusoidal forcing at a frequency different from the dominant mode, but the effect on the jet's actual penetration and spread is not significant. For this regime, strong periodic jet forcing with a prescribed time scale that is related to optimal vortex ring generation is required to impact visible jet penetration and spread.

I. Introduction

THE transverse jet or jet in crossflow (JICF) is a flowfield with widespread applications in energy and propulsive devices [1]. The ability to control the penetration and spread and/or mixing associated with this flowfield is highly beneficial, for example, in applications including fuel injection in high-speed aircraft engines, dilution jet injection in gas turbine combustors, thrust vectoring jets, and turbine blade film cooling. The JICF typically consists of a jet of mean velocity U_j issuing perpendicularly into a crossflow of velocity U_∞ , with the jet exiting either from a nozzle or orifice embedded within a wall or from an extruding pipe or nozzle. Typical parameters used to characterize this flowfield include the jet-to-crossflow velocity ratio $R \equiv U_j/U_\infty$ and the jet Reynolds number Re , which is based on the jet's inner diameter D . The fundamental dynamics of the JICF are dominated by a complex, interrelated set of vortex systems [2,3], among them the counter-rotating vortex pair (CVP), observed to dominate the jet's crossflow [4], shear layer vortices, whose rollup and deformation is thought to be associated with CVP formation [5], horseshoe vortices forming about jets introduced flush with respect to the injection wall [6], and wake vortices that are thought to draw fluid from the wall boundary layer into the jet [2]. A recent review article describes fundamental features of this flowfield [7].

Active forcing of jets in crossflow have been found to enable control of the penetration and mixing processes. Some recent studies have involved square-wave forcing of liquid jets in liquid crossflow, using fully modulated excitation [8] for moderately high jet-to-crossflow velocity ratios ($R = 5$ and 10). These studies suggest that forcing with low duty cycles ($\alpha \equiv \tau/T \sim 0.2$) can lead to deeply penetrating transverse jets with distinct vortex rings [9]. Other researchers exploring excitation of gaseous transverse jets, also at relatively high values of R (e.g., $R = 6$ [10]), find that even moderate

amplitudes of sinusoidal excitation (30% of the mean jet velocity), and at high frequencies compared with the preferred mode, can lead to improved transverse jet mixing and spread.

Prior experimental research on controlled transverse jets at the University of California, Los Angeles [11–14], has focused on acoustically forced, flush round jets with relatively low jet-to-crossflow velocity ratios, $R = 2.56$ and 4.0 . In contrast to others' observations at a higher R value [10], experiments with forced sinusoidal excitation of the jet at $R = 2.56$ in [12] show relatively little visual influence on jet response, even with very large amplitude excitation, exceeding 75% of the mean jet velocity, irrespective of the frequency of excitation. On the other hand, square-wave excitation of the jet at subharmonics of the unforced shear layer frequency, and with the same rms of the velocity excitation as in sinusoidal forcing, yields significant increases in the jet penetration and spread in many cases [12,14]. Distinct, deeply penetrating vortical structures are formed periodically in response to square-wave forcing, creating much greater overall jet penetration and, for low duty cycles, a bifurcated jet structure. The conditions (forcing frequencies, duty cycles for square-wave excitation, amplitudes of excitation) leading to enhancement of jet penetration and spread indicate that specific values of the temporal pulse width τ can provide optimal merger and penetration of vortical structures [14]. The time scales associated with this optimization appear to be nominally related to a universal time scale or nondimensional stroke ratio L/D associated with coherent vortex ring formation [15], which is observed to be optimized for L/D in the range 3.6–4.5.

Recent explorations of the transverse jet's shear layer instabilities have in part explained these differences in the type of excitation conditions producing improvements in jet penetration and spread. An extensive experimental examination of the instabilities associated with the isodensity transverse jet's near field upstream shear layer [16,17] in the range $1 < R \leq 10$ and with jet Reynolds numbers of 2000 and 3000, indicates significant differences in the nature of these instabilities, depending on the flow regime. When the crossflow is turned on, for a fixed jet Reynolds number, and R is reduced, shear layer instabilities at the upstream side of the jet are observed to be strengthened, to be initiated closer to the jet orifice, and to increase in frequency for the regime $3.3 \lesssim R \leq 10$. Results and trends in this regime are consistent with separate theoretical studies exploring the shear layer instabilities via linear stability analysis [18,19]. The experimentally observed instabilities in this regime also exhibit frequency shifting downstream as one moves along the jet shear layer for either nozzle configuration at these moderately high values of R . When R is reduced below about 3.3 for the flush injection and below 1.25 for the elevated jet experiments, single mode instabilities are

Presented as Paper 2008-0741 at the 46th AIAA Aerospace Sciences Meeting and Exhibit, Reno, NV, 7–10 January 2008; received 8 November 2009; revision received 21 February 2010; accepted for publication 11 April 2010. Copyright © 2010 by Juliet Davitian. Published by the American Institute of Aeronautics and Astronautics, Inc., with permission. Copies of this paper may be made for personal or internal use, on condition that the copier pay the \$10.00 per-copy fee to the Copyright Clearance Center, Inc., 222 Rosewood Drive, Danvers, MA 01923; include the code 0001-1452/10 and \$10.00 in correspondence with the CCC.

*Graduate Student Researcher, Department of Mechanical and Aerospace Engineering.

†Professor, Department of Mechanical and Aerospace Engineering.

‡Professor, Department of Mechanical and Aerospace Engineering; ark@seas.ucla.edu. Fellow AIAA (Corresponding Author).

dramatically strengthened, forming almost immediately after injection within the shear layer and with additional harmonics, in the absence of any evidence of frequency shifting.

This significantly altered character of the upstream shear layer spectra for these lower values of R , in addition to the fact that the shear layer is not affected by very low-level jet excitation when $R < 3.3$ for the flush jet and $R < 1.25$ for the elevated jet [16] provides evidence that the shear layer becomes absolutely unstable under these strong crossflow conditions. Further explorations of this transition [17] indicate other behaviors consistent with well-known canonical flows known to undergo transition to global instability, e.g., the low-density jet in quiescent surroundings [20–23] or the countercurrent mixing layer [24]. Shear layer spectra for globally unstable flows, where the natural disturbance is so strong that there is little energy transfer from a fundamental to a subharmonic mode, are not affected by low-level external excitation, as seen in the isodensity transverse jet [16]. But at higher amplitude sinusoidal jet excitation of a globally unstable flow, or when excitation is applied at lower amplitudes but at a frequency f_f that is very close to the unforced jet's dominant frequency f_o , the forcing frequency is observed to dominate shear layer behavior, producing a lock-in by the flow to the forcing condition and an absence of the natural behavior [17]. This behavior is well documented for the isodensity transverse jet in contour maps identifying regions of the frequency-amplitude space where the forcing frequency can overtake the global instability, and is similar qualitatively to observations for the globally unstable, low-density free jet [23,25]. Such sinusoidal excitation of the transverse jet is but one means of potential control.

These differences in the transverse jet's shear layer instability characteristics begin to explain the aforementioned differences in the response of transverse jets to forcing [10,12,14]. At the higher jet-to-crossflow velocity ratio explored in [10], the shear layer is likely convectively unstable and hence is strongly influenced by relatively low-level excitation. On the other hand, at the relatively low R values explored in [12,14], the flow is likely absolutely unstable, and hence introduction of large amplitude excitation with a distinct time scale (as can be achieved via temporal square-wave forcing) may be required to influence jet response. In these earlier transverse jet control studies, as noted earlier, no substantial response to strong sinusoidal forcing is observed.

The shear layer instability characteristics suggest that flow regime-dependent forcing strategies could be applied to control such jets in practical systems. For example, one could postulate that relatively low-level sinusoidal excitation could be employed to promote mixing when the transverse jet is undergoing convective instability, for higher R values. On the other hand, at lower values of R , where the unforced JICF exhibits self-excited behavior, a different type of forcing is required to be able to affect penetration and spread. While the earlier results for transverse jet excitation at lower R values [12,14] suggest that high-amplitude square-wave excitation, especially with a distinct timescale related to vortex ring formation [15], may be required to impact jet penetration and spread, the above-mentioned JICF instability experiments [17] indicate that very strong sinusoidal excitation of the globally unstable transverse jet, and/or low or moderate excitation at frequencies f_f close to the natural self-excited frequency f_o , can at least affect the shear layer, if not the jet itself. Hence the optimal means by which the transverse jet is controlled may well depend on the flow regime (with respect to R value). The purpose of the present study is to explore the impact of this sort of two-pronged strategy in the control of transverse jet penetration and spread.

II. Experimental Methods

A. Setup and Procedures

Figure 1 provides a schematic diagram of the experimental setup used in this and prior studies for a nitrogen jet injected transversely into a crossflow of air. The wind tunnel test section was 12 by 12 cm in cross section, with a tunnel length four times that shown in Fig. 1. Crossflow speeds upstream of the jet ranged from 1.3 to 7.2 m/s, with turbulence intensities less than 1.5%. Two different jet nozzles were used, each with an exit inner diameter of 0.4 cm, created by a smooth fifth-order polynomial contraction. One jet was positioned flush with respect to the wind tunnel floor and the other was elevated from the injection wall by 3.75 jet diameters, the exit of which was well outside of the injection wall boundary layer.

A single component hot-wire anemometer (Dantec 55P15) was used to characterize the velocity field and spectral character of the vertical disturbance velocity in the jet shear layer. Hot-wire output signals were acquired by a dynamic signal analyzer (HP-35665A),

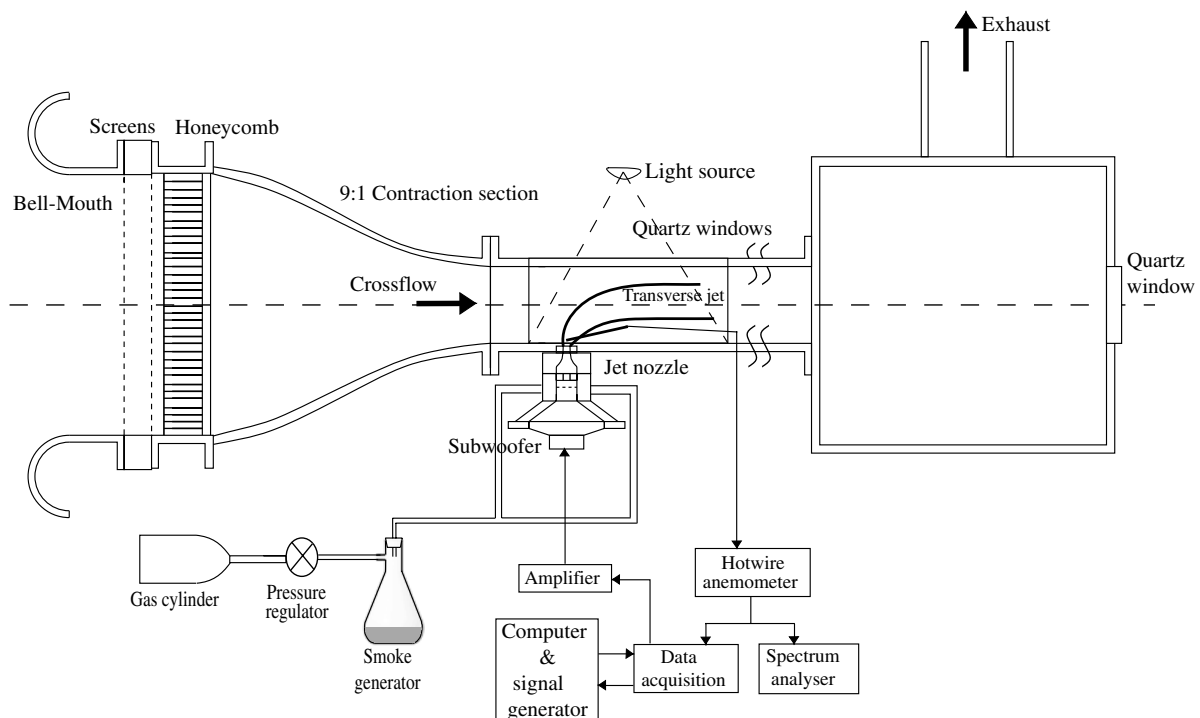


Fig. 1 Schematic diagram of the low-speed wind tunnel and associated transverse jet excitation apparatus. The actual tunnel had three additional sections situated downstream of the one shown, of identical dimensions.

capable of capturing frequencies of up to 25 kHz, and a high-speed data acquisition system to enable the acquisition of power spectra and temporal jet response. The hot-wire was calibrated in the wind tunnel with respect to the crossflow using a Dwyer pitot probe and two Omega Engineering (PX653-03D5V and PX653-0.25D5V) differential pressure transducers. Calibrations were performed regularly to ensure accurate jet and crossflow velocity conditions. A loudspeaker situated below a small plenum section was connected to the nozzle; the speaker, driven by a signal generator and amplifier, acted to excite the jet flow according to the desired (actively controlled) temporal waveform. For most operating conditions with $R > 3.5$, top hat-like spatial velocity profiles with thin boundary layers were produced at the jet exit, as quantified in [16]. While experiments at jet Reynolds numbers Re of 2000 and 3000 are described in [16], showing similar shear layer stability characteristics, only $Re = 2000$ jets were explored in the present jet excitation studies.

Visualization of the JICF was achieved via smoke generation upstream of the jet nozzle/plenum, providing a method to observe jet differences with alternative forcing conditions. Seeding of the jet was accomplished by having the nitrogen pass through a heated seeder with a liquid paraffin solution. The jet fluid line downstream of the seeder was cooled to ensure jet temperatures equal to that of the crossflow. The top and adjacent sides of the test section were fitted with quartz windows, and a 500 W white light was used to illuminate the seeded jet. A digital Nikon D100 camera capable of producing digital ISOs of 200–6400 and shutter speeds of 30 – 1/4000 s captured long and short exposure smoke images. While smoke visualization, as a line of sight imaging method, did not allow detailed quantification of mixing, long exposure smoke images ($\approx 1/15$ s) could be used to quantify the effectiveness of different forcing conditions in enhancing overall jet spread and penetration, while short exposure images ($\approx 1/4000$ s) were used to examine dominant jet structures.

The Canny edge detection method [26] was used via MATLAB's image processor to detect and characterize the boundary/edge of the seeded jet by determination of maxima in pixel gradients. To quantify the spread enhancement of the forced JICF, the coordinates of the upper and lower trajectories were subtracted, producing the quantified jet spread, $\delta(x)$, for different x/D (downstream) locations. When the edge detection algorithm was applied to smoke images for the flush nozzle at very low R values, a significant number of false edges were detected because the lower part of the smoke-seeded jet was very close to the lower tunnel wall. A manual process was required in those cases to select the edge/boundary of the upper and especially the lower edges of the jet. Uncertainties in spread and penetration measurements arose from the difficulty in selecting the boundaries of the jet, especially for low R values; for these latter conditions, this uncertainty was as high as 8%, whereas for the higher R values it was smaller, of the order of 2% [17].

B. Waveform Feedforward Controller

In prior [12,14] as well as current jet forcing experiments, the desired temporal input signal to the loudspeaker in Fig. 1, either a sine or square-wave, was delivered by a signal generator/spectrum analyzer through an amplifier. The hot-wire anemometer placed at the center of the exit plane of the jet enabled measurement of the actual temporal waveform that was produced. Comparison of the hot-wire output and the input signal allowed the dynamics of the system to be characterized, with evidence of an alteration to the jet velocity's temporal waveform that significantly differed from the input waveform. A digital signal processor (DSP) was used to preshape the amplifier's reference command so that the resulting temporal profile of the jet velocity perturbation more closely resembled the desired waveform.

In previous studies [12,14] the DSP filter was designed after identifying models of the actuator dynamics at different operating points, and then essentially inverting this model in a causal manner. The result was that a pulse input to the DSP filter could be reproduced, with a time delay, in the jet velocity at the jet exit. The design process for this controller was arduous, however, and involved

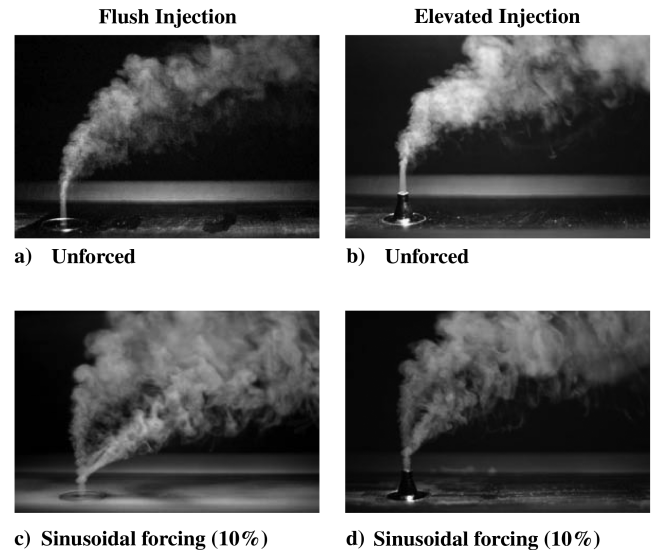


Fig. 2 Smoke visualization of the transverse jet for $R = 10$, with an exposure time of 1/4000 s, shown for both flush and elevated injection: a–b) without jet excitation and c–d) with sinusoidal jet forcing at frequency $f_f = 0.1f_o$ such that the excitation velocity is approximately 10% of the mean jet velocity.

high-order models (30 to 40 states) of the actuation system which were subsequently reflected in high-order DSP filters due to the model matching filter synthesis technique. Although for the relatively low R cases explored in [12,14] this approach is successful, the procedure required significant tuning at each operating point, i.e., at each jet and crossflow condition.

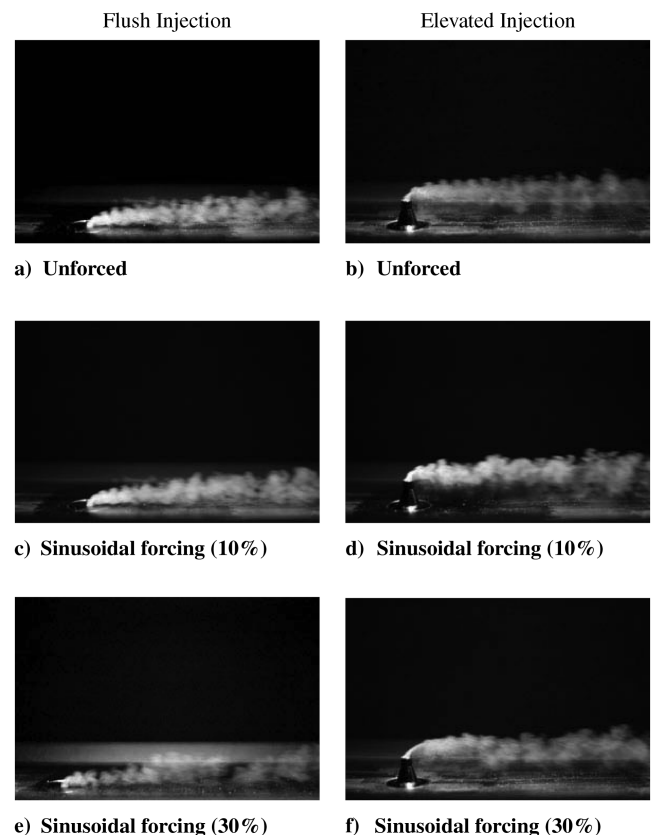


Fig. 3 Smoke visualization of the transverse jet for $R = 1.15$, with an exposure time of 1/4000 sec, shown for both flush and elevated injection: a–b) without jet excitation, c–d) with sinusoidal jet forcing at frequency $f_f = 0.1f_o$ such that the excitation velocity is approximately 10%, and e–f) 30% of the mean jet velocity.

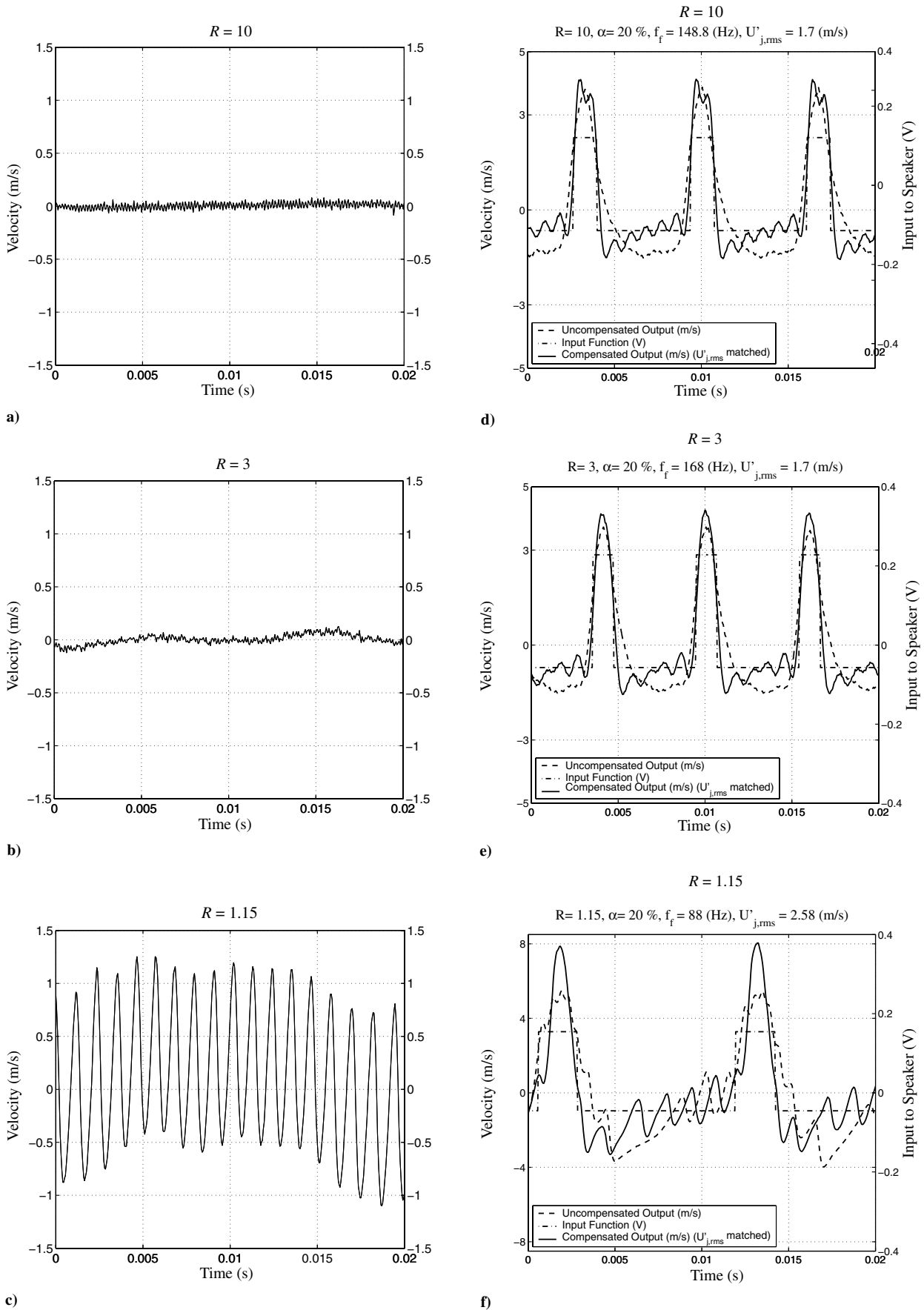


Fig. 4 Temporal waveforms measured at the center of the flush transverse jet's exit plane: a–c) waveforms for $R = 10, 3, 1.15$, respectively, in the absence of external forcing, and d–f) corresponding waveforms at the same R values for the effect of applied square-wave forcing at frequency $f_f = 0.10f_0$ and duty cycle 20%. Shown are the input voltage waveform to the actuator (dash-dotted, V) and the mean-subtracted velocities at the center of the jet exit plane without control (dashed line, m/s) and with control (solid line, m/s). $U'_{j,rms}$ is matched between the controlled and uncontrolled cases.

An alternative control procedure was adopted in the present study, in particular for the low jet-to-crossflow velocity ratios creating globally unstable or self-excited shear layers. This procedure was based on the recognition that a periodic jet perturbation was typically desired in these jet forcing experiments, and because of this, the general model inversion approach of our prior research was not necessary, since only knowledge of the actuator dynamics at the fundamental frequency f_o and its harmonics (the Fourier series components of the desired square waveform) was required. Thus, in the present study, once the desired jet velocity perturbation was specified, the dynamics of the actuator were identified only at the fundamental frequency f_o and a handful of harmonics. Because of the actuation system's bandwidth limitation to about 1 kHz, if the desired temporal waveform for jet forcing had a fundamental frequency f_f near 100 Hz, for example, then the first 10 components of its Fourier series could be faithfully reproduced in jet velocity. It was on this grid of Fourier series frequencies that the actuator frequency response was identified using a correlation technique [27].

The input to the speaker amplifier consisted of the summed outputs of a series of sine-wave generators (generated by the DSP) whose frequencies were set to the Fourier series frequencies below actuator's 1 kHz cutoff frequency. With knowledge of the actuator frequency response and the desired velocity perturbation Fourier series, the magnitude and phase of each sine-wave was adjusted so that after filtering by the actuator, the truncated Fourier series of the desired velocity waveform was recovered at the jet exit. This process was easily automated and lent itself to rapid experimentation under a range of conditions during the present transverse jet experiments. Of course, since this approach to actuator compensation did not use feedback, it could not compensate for other disturbances in the jet velocity, and hence the output waveform did not completely reproduce the desired input waveform, especially during the conditions at low R values, producing global instability. Nevertheless, the overall improvement in the compensated square waveform compared with the uncompensated waveform enabled a more accurate exploration of the effect of square-wave forcing parameters on jet behavior, which will be discussed in Sec. III.A.

III. Results

A. Response to Sinusoidal and Square-Wave Forcing

Earlier studies [16] on the transverse jet shear layer instabilities indicate that very low-level sinusoidal forcing of the jet at frequency f_f (with amplitude less than 1% of the mean jet velocity) causes excitation of a dominant mode at the applied frequency f_f , and reduction or elimination of the natural fundamental disturbance at frequency f_o , when $R \gtrsim 3.5$ for the flush jet and when $R > 1.2$ for the elevated jet, consistent with a convectively unstable flow. For the lower values of R creating globally unstable flow ($R \lesssim 3.3$ for the flush jet and $R \lesssim 1.2$ for the elevated jet), very low-level forcing shown in [16] has little effect on the shear layer. Further explorations in [17] indicate that stronger sinusoidal excitation of the jet at a frequency f_f for $R < 3.5$ can overtake the dominant frequency associated with the global instability at f_o , and can do so at lower amplitude excitation if f_f is close to f_o . In fact, if $0.9 \lesssim f_f/f_o \lesssim 1.1$, forcing amplitudes at or below 5% of the mean jet velocity allow f_f to completely dominate the shear layer spectra. In other transverse jet cases, moderate sinusoidal forcing with perturbation velocity amplitudes between 10 and 30% of the mean jet velocity and for $f_f < 0.9$ produce spectra where the peak at f_o is still present but where f_f is dominant. This type of behavior is well-established for other globally unstable flows, as seen experimentally for the low-density free jet [23,25], based on theoretical ideas on the control of absolutely unstable flows [28]. The observation is consistent with the nature of a Hopf bifurcation in an instability to a global mode, as outlined in [29]. It is of interest in the present paper to determine if such strong sinusoidal forcing has an appreciable effect on jet penetration and spread when the jet is absolutely unstable, in contrast to the effects of square-wave excitation previously explored to a limited degree [12,14].

The effects of sinusoidal jet excitation on visible jet structure for high ($R = 10$) and low ($R = 1.15$) jet-to-crossflow velocity ratios are shown in Figs. 2 and 3, respectively, for both flush and elevated jets. In each figure, the root-mean-square of the jet excitation velocity amplitude, $U'_{j,rms}$, was matched for the corresponding cases with forcing. At $R = 10$ for both flush and elevated jets, excitation at 10% of the mean jet velocity produced considerable increases in jet spread and slight improvements in penetration of the upper portion of the jet. In contrast, when this moderate sinusoidal forcing was applied to the jet for $R = 1.15$ (Figs. 3c and 3d), relatively little alteration to the shear layer instability or to the jet itself was observed (i.e., compared with Figs. 3a and 3b). Even when the forcing amplitude was increased to 30% of the mean jet amplitude, indicated in Figs. 3e and 3f for the flush and elevated jets, respectively, the external forcing had a minimal influence on the jet's overall behavior. For such sinusoidal forcing at a frequency f_f much lower than f_o , there was evidence of a slight modulation of the jet's vortical structures, e.g., for the flush jet in Fig. 3e, but there was no substantial alteration to the flow or overall penetration. Thus, despite the fact that the spectral data indicate that the forcing frequency f_f overtakes the shear layer instability for this relatively high-amplitude forcing [17], there appeared to be little effect on jet structure, penetration, and spread. In contrast, low-to-moderate jet forcing had visible impact on the flowfield when R was large, consistent with a convectively unstable shear layer.

Temporal square-wave forcing was then explored in these experiments, allowing the introduction of an additional time scale to the flowfield, the temporal pulse width, τ , as done in prior forced transverse jet experiments [12,14]. Square-wave forcing at a prescribed frequency f_f (or period T) and duty cycle $\alpha = \tau/T$ allowed generation of the specific temporal pulse width, τ .

Table 1 For different input duty cycles α_{input} , the actual duty cycle α_{actual} and the actual L/D value for the flush transverse jet^a

$\alpha_{input}, \%$	$R = 10$		$R = 3$		$R = 1.15$	
	$\alpha_{actual}, \%$	L/D	$\alpha_{actual}, \%$	L/D	$\alpha_{actual}, \%$	L/D
2	13.1	2.7	15.2	2.8	8.5	3.2
5	13.2	2.8	15.2	2.8	8.9	3.3
10	14.3	3.0	16.0	2.9	9.5	3.6
15	20.4	4.2	18.9	3.4	23.1	6.9
20	25.3	5.0	26.6	4.6	24.2	7.3
25	29.3	5.7	30.9	5.2	26.0	7.9
30	35.5	6.7	34.4	5.7	26.6	8.0
35	39.2	7.3	40.9	6.6	35.4	10.1
40	44.6	8.1	45.4	7.3	38.2	10.8
45	50.8	9.1	49.8	7.8	38.6	10.7
50	54.5	9.6	56.5	8.7	47.7	12.8

^aForcing frequencies of $f_f = 0.10f_o$ are applied for each R value, with an approximate amplitude of 30%.

Table 2 For different input duty cycles α_{input} , the actual duty cycle α_{actual} and the actual L/D value for the elevated transverse jet^a

$\alpha_{input}, \%$	$R = 10$		$R = 3$		$R = 1.15$	
	$\alpha_{actual}, \%$	L/D	$\alpha_{actual}, \%$	L/D	$\alpha_{actual}, \%$	L/D
2	12.7	2.6	17.7	2.8	-	-
5	12.7	2.6	17.8	2.8	9.1	3.7
10	13.6	2.8	18.2	2.9	13.7	5.0
15	20.8	4.1	20.1	3.1	16.4	6.1
20	25.6	4.9	26.8	4.0	22.1	7.3
25	28.7	5.4	34.4	4.9	21.9	7.5
30	35.4	6.4	37.4	5.3	27.4	9.0
35	39.5	7.0	42.1	5.9	35.1	10.6
40	44.6	7.8	48.0	6.5	38.2	11.9
45	51.8	8.8	54.9	7.3	40.6	12.3
50	54.8	9.2	58.3	7.7	45.1	13.4

^aForcing frequencies of $f_f = 0.10f_o$ are applied for each R value, with an approximate amplitude of 30%.

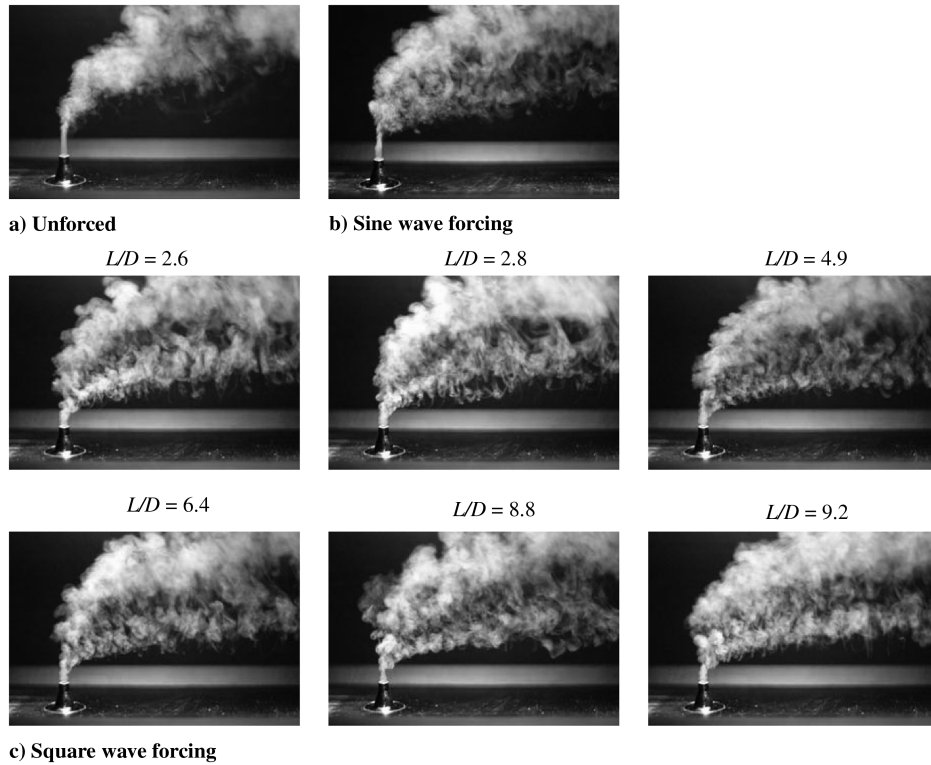


Fig. 5 Smoke visualization of the elevated transverse jet for $R = 10$: a) no forcing, b) sinusoidal forcing ($f_f = 0.10f_o = 147.2$ Hz), and c) square-wave forcing ($f_f = 0.10f_o$) with increasing input duty cycles and corresponding actual L/D values. $U'_{j,rms} = 1.7$ m/s was matched among all forcing cases. Images are shown with an exposure time of 1/4000 s.

Application of the feedforward controller described in Sec. II enabled studies to be performed which compared the behavior of forced transverse jets under different excitation conditions, e.g., sinusoidal and square-wave forcing, but with the rms of the net

velocity excitation, $U'_{j,rms}$, matched. Matching the rms among different excitation conditions allowed the same effective impulse to be delivered to the jet, so that the effects of waveform and time scales could be understood more systematically.

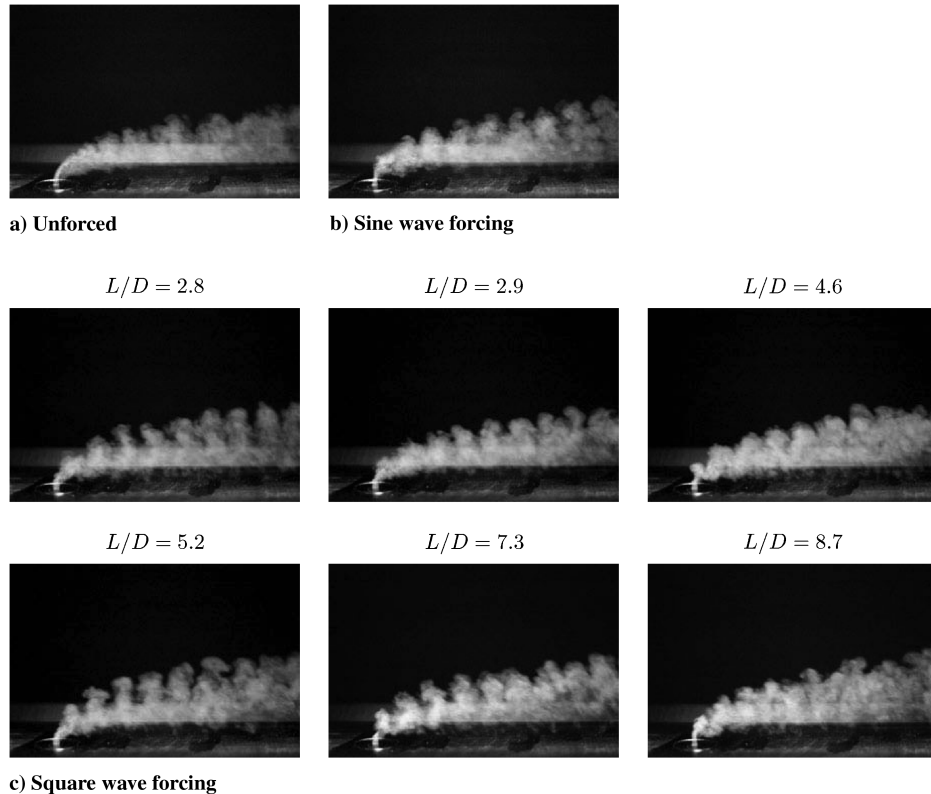


Fig. 6 Smoke visualization of the flush transverse jet for $R = 3$: a) no forcing, b) sinusoidal forcing ($f_f = 0.10f_o = 168$ Hz), and c) square-wave forcing ($f_f = 0.10f_o$) with increasing input duty cycles and corresponding actual L/D values. $U'_{j,rms} = 1.7$ m/s was matched among all forcing cases. Images are shown with an exposure time of 1/4000 s.

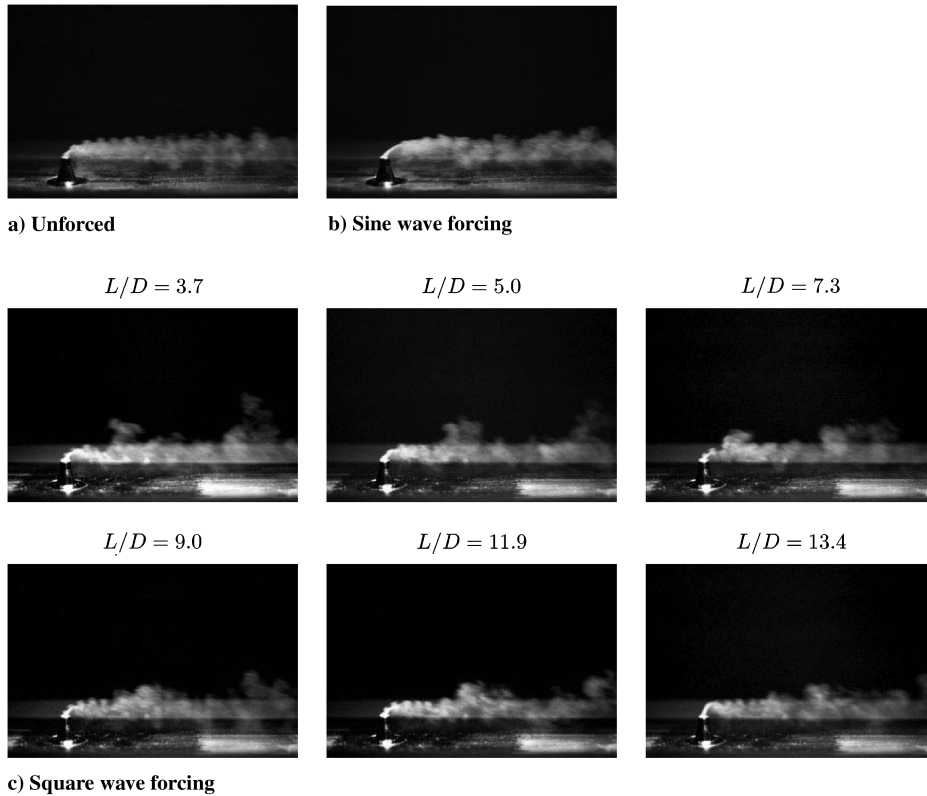


Fig. 7 Smoke visualization of the elevated transverse jet for $R = 1.15$: a) no forcing, b) sinusoidal forcing ($f_f = 0.10f_o = 88$ Hz), and c) square-wave forcing ($f_f = 0.10f_o$) with increasing input duty cycles and corresponding actual L/D values. $U'_{j,rms} = 2.58$ m/s was matched among all forcing cases. Images are shown with an exposure time of 1/4000 s.

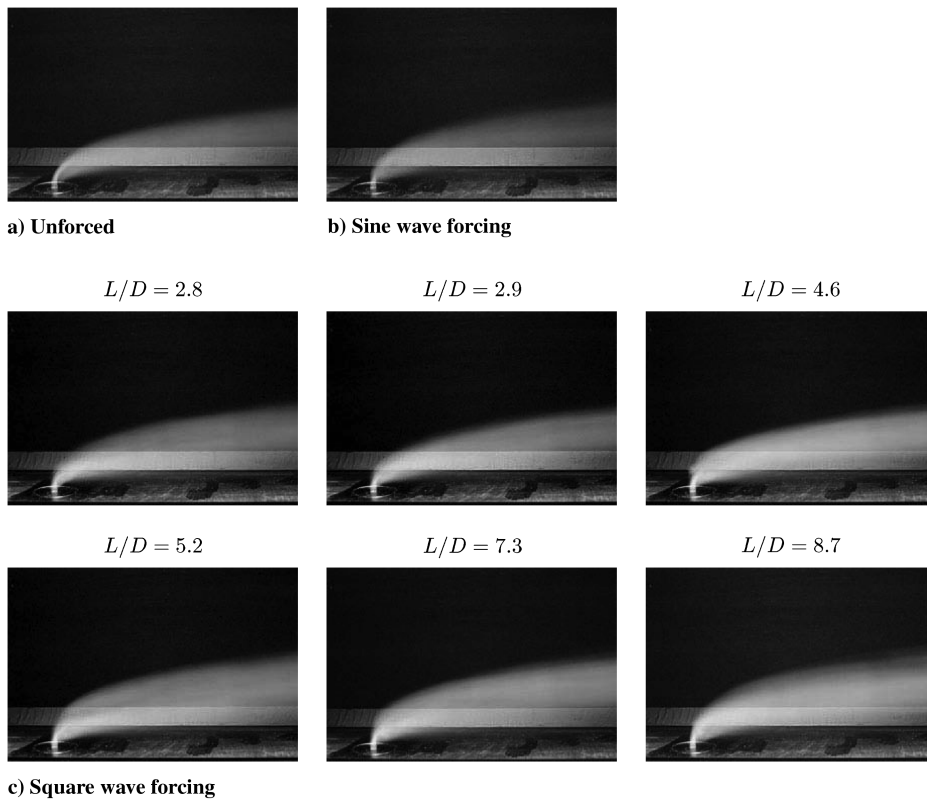


Fig. 8 Smoke visualization of the flush transverse jet for $R = 3$ with long exposures: a) no forcing, b) sinusoidal forcing ($f_f = 0.10f_o = 168$ Hz), and c) square-wave forcing ($f_f = 0.10f_o$) with increasing input duty cycles and corresponding actual L/D values. $U'_{j,rms} = 1.7$ m/s was matched among all forcing cases. Images are shown with an exposure time of 1/15 s.

Because the actuation system bandwidth was limited to approximately 1000 Hz, square-wave forcing at relatively low frequencies, close to 100 Hz, was typically employed in order that the first 10 components of the Fourier series could be used to reproduce the desired square waveform. The effects of the controller on the temporally evolving waveforms at the center of the flush transverse jet's exit plane for $R = 10$, 3, and 1.15 are shown in Fig. 4, with the mean velocity subtracted. Data in Figs. 4a–4c were measured at different R values in the absence of external forcing, providing evidence of the very strong instability at a single frequency for $R = 1.15$. Although the upstream and side shear layers for the flush jet at $R = 3$ exhibit a strong instability consistent with globally unstable flow, the peak at the center of the jet exit's spectra corresponding to Fig. 4b is not as strong [17]. The effects of square-wave forcing were then explored in the present tests at a frequency $f_f = 0.1f_o$, with results in Figs. 4d–4f for the input (desired) square waveform and the measured output waveform, with and without the application of the controller. In all excitation cases shown, the rms of the net velocity excitation, $U'_{j,rms}$, was matched for a given R condition.

The principal benefit of the controller was to allow formation of a clear upsweep, discernible pulse width, and clear downsweep in the waveform, with a pulse width closer to that of the input signal. Although there was still a considerable degree of ringing in the compensated waveforms, particularly when the jet was already

globally unstable as for $R = 1.15$ in Fig. 4f, there was nevertheless an improvement in the pulse width over the more sinelike waveform created in the absence of control.

The waveforms such as those in Figs. 4d–4f were sufficient to be able to study the effect of excitation with a characteristic time scale. At higher duty cycles ($\alpha > 20$ –25%), the input (desired) and controlled output waveforms were relatively close to 1 another, but at lower duty cycles there was a greater discrepancy between the two. These differences between input and output waveforms manifested themselves in differences between the input or desired duty cycle $\alpha_{input}(=\tau_{input}/T)$ and the output or actual duty cycle $\alpha_{actual}(=\tau_{actual}/T)$. A method for quantifying these differences was devised, based on the 5% criterion used in [8]. This criterion quantifies the actual pulse width, τ_{actual} , as the temporal width of a signal measured from a point at 5% of the average peak velocity amplitude, starting above the minimum point before the upsweep in signal occurs. The actual (calculated) pulse width can then be used to approximate the effective nondimensional stroke length for square-wave excitation, L/D , which is comparable to the universal time scale concept for vortex ring formation as described by [15]. The expression for L/D in the present configuration takes the form

$$\frac{L}{D} = \frac{1}{D} \int_0^{\tau} u_j dt \quad (1)$$

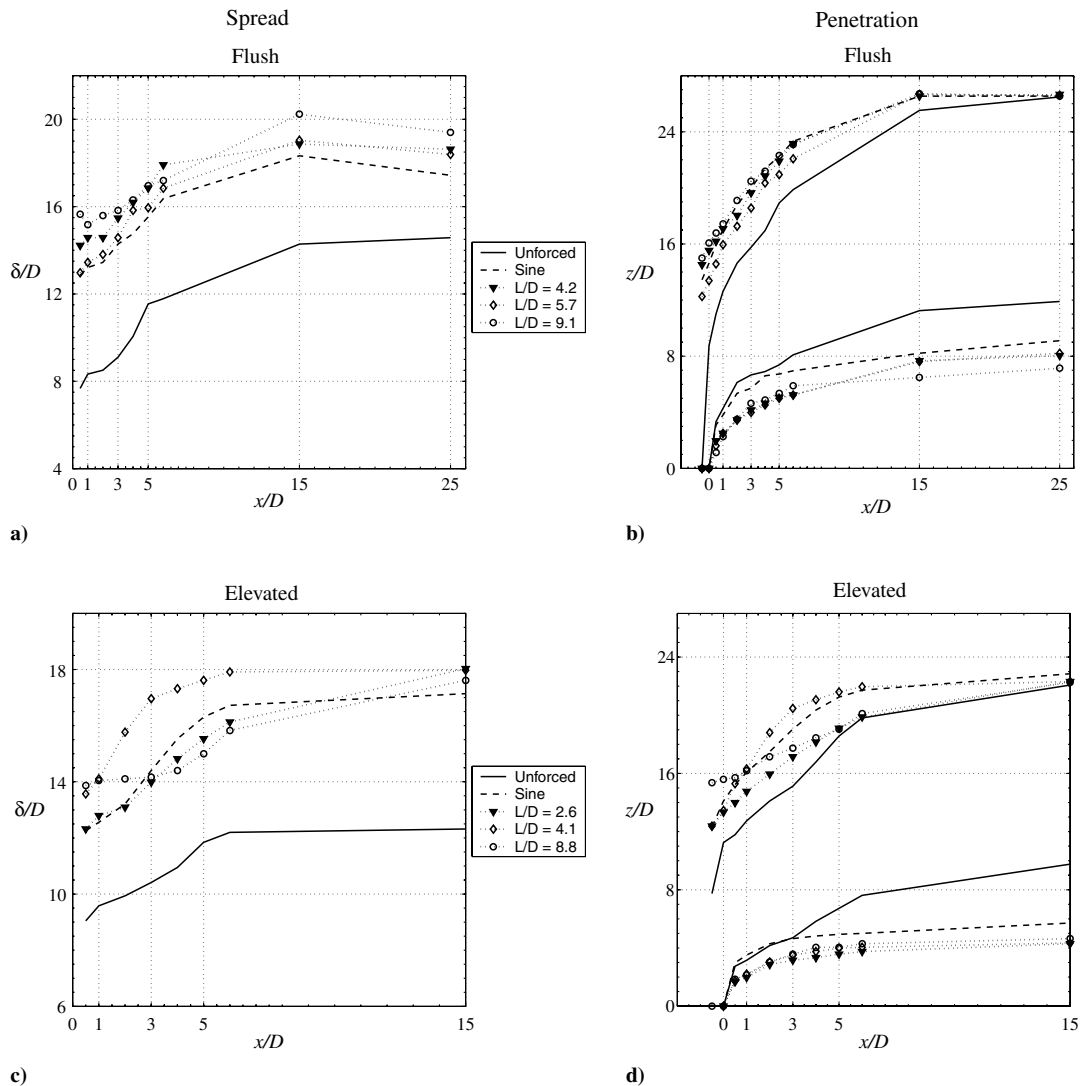


Fig. 9 Spread and penetration quantification for $R = 10$: a) spread quantification for flush transverse jet, b) penetration quantification for flush transverse jet, c) spread quantification for elevated transverse jet, and d) penetration quantification for elevated transverse jet. Unforced cases are shown with solid lines, sinusoidal forcing with dashed lines, and square-wave forcing results with corresponding L/D values are shown with symbols.

Thus for the various cases explored in the present study (flush and elevated jets, different R values, different forcing frequencies f_f and duty cycles α for square-wave excitation), the various input duty cycles produced different actual duty cycles compared with the input α , influencing the nondimensional stroke length L/D . These differences are tabulated in Tables 1 and 2 for the flush and elevated jets, respectively, at various R values. Clearly, for input duty cycles below about 20–25%, there were moderate to large differences between desired (input) and actual duty cycles, even with the feedforward controller. Fortunately, the actual nondimensional stroke lengths spanned a range of L/D values of interest, so that a systematic study of critical length and timescales could be conducted with ease.

The effect of relatively strong square-wave excitation at approximately 30% of the mean jet velocity was explored in detail using the controller. Smoke visualization was performed to examine the effect of pulse width and hence L/D on visible jet response to such forcing by sweeping through input duty cycles α_{input} ranging from 2 to 50%. Extensive sets of short time exposure images are provided in the Ph.D. dissertation of Davitian [17], with sample results shown in Figs. 5–7 or $R = 10, 3$, and 1.15, respectively. A set of longer exposure images for $R = 3$ is shown in Fig. 8, for comparison with images under the same conditions in Fig. 6. In each of these figures (Figs. 5–8), the unforced transverse jet image is shown in part a, images with sinusoidal forcing are shown in part b,

and the effects of square-wave forcing at different duty cycles, and hence different L/D values, are shown in the multiple images in part c. In these sets of figures, $U'_{j,rms}$ was matched for all the forcing conditions shown for each R value. Quantification of the optimum spread and penetration via an edge detection image processing technique, for all forcing frequencies and amplitudes explored, will be discussed in Sec. III.B.

For the $R = 10$ elevated forced jet, shown in Fig. 5, the jet spread was significantly enhanced by high-amplitude sinusoidal forcing as compared with the unforced jet, an expected behavior for a convectively unstable flow. In comparison, square-wave forcing offered even greater spread, indicated by the images in Fig. 5c. In some cases the jets appeared more strongly bifurcated with square-wave forcing, especially at the lower duty cycles, but this would be expected based on the value of α and the resulting distribution of high and low momentum fluid. Interestingly, for the elevated jet as well as the flush jet (not shown) at $R = 10$ and with input duty cycles $\alpha_{\text{input}} = 40\text{--}50\%$, there was evidence of upstream-propagating vortex rings, as seen in Fig. 5c for $L/D = 8.8$. Structures appeared to be similar to those seen in bifurcated and blooming free jets [30].

Corresponding short exposure smoke images for the flush jet with $R = 3$ (shown in Fig. 6), for which the unforced jet is absolutely unstable [16,17] suggest that high-amplitude square-wave forcing had the effect of creating more distinct vortical structures as compared with the jet's unforced flow structures (Fig. 6a) and those

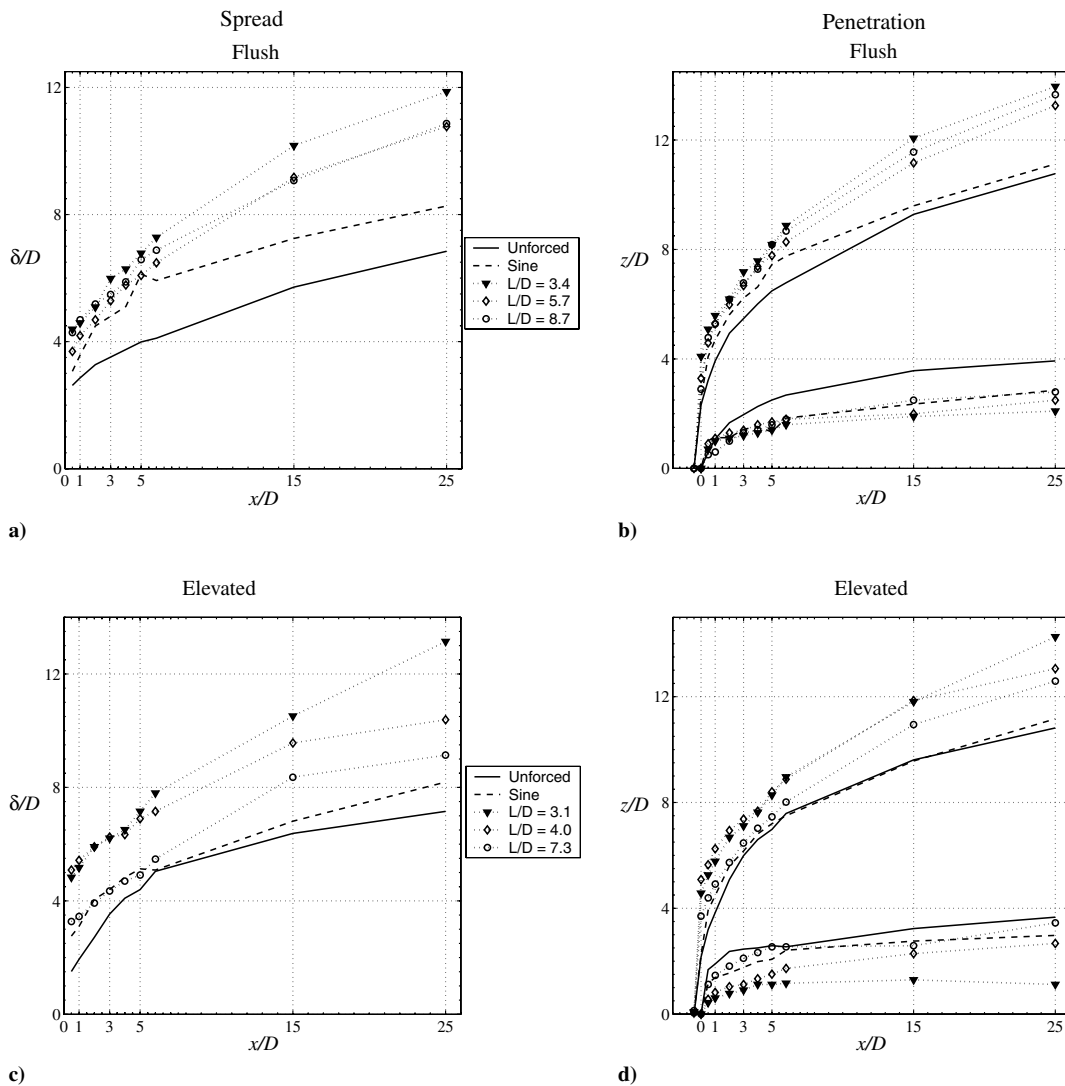


Fig. 10 Spread and penetration quantification for $R = 3$: a) spread quantification for flush transverse jet, b) penetration quantification for flush transverse jet, c) spread quantification for elevated transverse jet, and d) penetration quantification for elevated transverse jet. Unforced cases are shown with solid lines, sinusoidal forcing with dashed lines, and square-wave forcing results with corresponding L/D values are shown with symbols.

created by sine-wave forcing (Fig. 6b). Specific square-wave forcing conditions created rather deeply penetrating vortical structures that increased the overall spread of the jet. For example, $L/D = 2.8$ or 5.2 seemed to produce more distinct vortical structures with relatively good penetration. Longer exposure (1/15 sec) smoke images corresponding to those for $R = 3$ in Fig. 6 are shown in Fig. 8. These show that the optimum vortical structures for the range of conditions explored corresponded to higher penetration and spreading in the jets. For $R = 3$ these larger penetration cases tended to be observed for input duty cycles smaller than 30%, corresponding to the range $L/D \approx 2-5$. Sinusoidal forcing had a somewhat lesser influence for the flush jet at $R = 3$, consistent with the flow having become globally unstable [16,17].

Smoke images for the elevated jet with $R = 1.15$, shown in Fig. 7, reveal the potential benefits of square-wave forcing for a globally unstable flow. While sinusoidal forcing at a frequency considerably lower than the natural mode appeared only to slightly modulate the jet shear layer and trajectory, square-wave forcing produced stronger, periodic pulses of vorticity. These vortical puffs had the effect of increasing the overall penetration and spread of the jets. Interestingly, the relatively low momentum fluid that emerged from the jet orifice during the off period of the square-wave forcing appeared to cause the $R = 1.15$ jet to adhere more closely to the injection wall than during the unforced condition. This phenomenon could explain observations in others' experiments on low momentum ratio pulsed

cooling jets in hot crossflow [31,32], which determine that improved heat transfer effectiveness is obtained during square-wave excitation at lower duty cycles. When the overall mean velocity ratio R is fixed at a very low value, the present results suggest that square-wave forcing at low duty cycles could lower the bottom edge of the transverse jet, leading to increased transport to the wall.

B. Jet Penetration and Spread Quantification

Long exposure smoke images such as those in Fig. 8 were used to quantify overall jet penetration (upper and lower trajectories) and spread ($\delta(x)$) for forced and unforced jets in crossflow. The Canny image edge detection algorithm described in Sec. III.B was used in images such as those in Fig. 8 to track the upper and lower edges of the jet and to quantify edge trajectories and jet spread at different downstream locations x/D .

Figures 9–11 show spread and penetration data for $R = 10, 3$, and 1.15 , for both the flush and elevated nozzles, and for unforced and sinusoidally forced jets and for jets with square-wave excitation. A wide range of L/D values was explored, even for L/D values not shown in Figs. 5–11, but only representative values are shown in these latter figures to enable clearer distinctions among results. Full datasets for the range of L/D values explored may be found in the Ph.D. dissertation of Davitian [17]. For each flow condition in these figures, $U'_{j,rms}$ was matched. For $R = 10$, shown in Figs. 9a–9d the

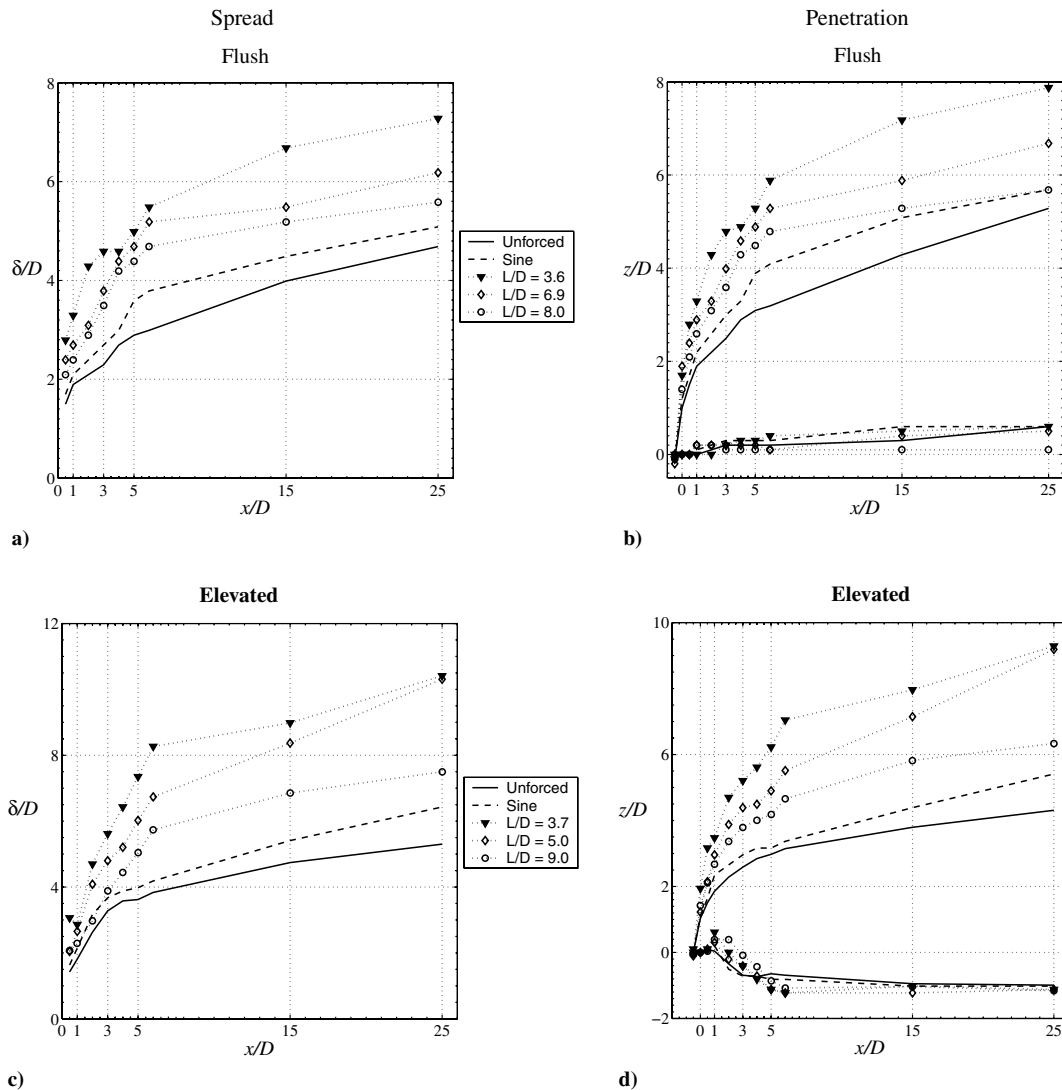


Fig. 11 Spread and penetration quantification for $R = 1.15$: a) spread quantification for flush transverse jet, b) penetration quantification for flush transverse jet, c) spread quantification for elevated transverse jet, and d) penetration quantification for elevated transverse jet. Unforced cases are shown with solid lines, sinusoidal forcing with dashed lines, and square-wave forcing results with corresponding L/D values are shown with symbols.

flush and elevated nozzles, respectively, spread and penetration of the jet were significantly enhanced in response to either sine or square-wave forcing. Quantitatively, all forced jets showed increased spread over the unforced condition; for both flush and elevated jets, edge trajectory tracking showed the upper edge moving upward as well as the lower trajectory of the jet moving downward. This quantification of spread and penetration for $R = 10$ showed that sine-wave forcing was generally as effective as square-wave forcing in enhancing spread and penetration compared with the unforced case.

In contrast, when the transverse jet was globally unstable, jet penetration and spread resulting from square-wave forcing had a much greater effect. Quantification for $R = 3$, shown in Figs. 10a–10d for the flush and elevated jets, respectively, and for $R = 1.15$, shown in Figs. 11a–11d, revealed significant differences between the effect of sinusoidal and square-wave forcing. While strong sinusoidal forcing was demonstrated via spectral characteristics in [17] and via smoke visualization in Figs. 6–8 to influence the transverse jet at these relatively low R values, square-wave forcing had a much greater impact. This was even the case for the elevated jet at $R = 3$, which was not globally unstable in the absence of forcing. L/D values creating maximum jet penetration and spread during square-wave forcing for $R = 3$ and 1.15 were in the range 3.1 to 3.7 for both the flush and elevated jets. As noted previously, the experiments of Gharib et al. [15] for a piston-generated vortex ring suggest optimal ring formation and propagation for L/D in the range of 3.6–4.5. The mechanism for enhanced jet spread is likely a direct result of the optimized vortex penetration by the forced transverse jets, achieved by the introduction of vorticity via relatively distinct temporal square-wave excitation.

IV. Conclusions

The differences in the stability characteristics of the shear layer for the JICF suggest a clear strategy for the control of jet penetration and spread. The benefits of a two-pronged, strategic approach to jet control, whereby the optimal type of temporal jet forcing depends on the value of R , were demonstrated in the present study. When the jet's shear layer exhibited convectively unstable characteristics, as observed for $R > 3.3$ for the flush jet and $R > 1.2$ for the elevated jet, low-to-moderate sinusoidal forcing produced a measurable increase in jet penetration and spread. Examples of this behavior are shown in Figs. 5 and 9. In contrast, such forcing, even at a high amplitude, appeared to have a relatively minimal or no effect on jets in the $R \lesssim 3.3$ regime for the flush jet or $R \lesssim 1.2$ for the elevated jet, where the shear layer exhibits globally unstable behavior. This result is interesting in the sense that other globally unstable flows exhibiting lock-in do generally see the ability to influence flow behavior, e.g., low-density jet spread, via sufficiently strong sinusoidal excitation upstream of the initiation of the instability [23,25].

In the present transverse jet experiments under globally unstable unforced conditions, as shown in Figs. 6–8, 10, and 11, strong square-wave forcing at lower duty cycles, in many cases with a prescribed temporal pulse width that corresponds to optimal vortex ring formation and penetration ($L/D \approx 3.1$ to 3.7) was required to impact jet behavior. Although the temporal waveforms in the present paper were not precise square waves, recent direct numerical simulations of the pulsed transverse jet by Sau and Mahesh [33] suggest that the types of imperfections seen in the present study and in [14] have a negligible effect on transverse jet evolution when compared with exact square waves with the same pulsewidth. The relatively deeply penetrating vortical structures seen in the smoke images here and in [17] are similar to those seen in the computations, and suggest that operating parameters may have been close to optimal conditions. The fact that the forcing conditions in these images were associated with stroke ratios L/D of the order of four, consistent with data in [15] for optimal vortex ring formation, lends credence to the conclusions of [14] on the relevance of vorticity generation for maximized jet penetration. Clearly, the control of some globally unstable flows, such as the transverse jet, requires a more physics-based strategy than can be accomplished by high

amplitude, sinusoidal excitation in order to achieve significant flow response.

Acknowledgments

Support for this project from the National Science Foundation under grants CTS-0457413 and CBET-0755104, and from the NASA Graduate Student Research Program is gratefully acknowledged. The authors wish to acknowledge helpful discussions with Robert Kelly of the University of California, Los Angeles; and Leonardo Alves of the Instituto Militar de Engenharia, Rio de Janeiro, Brasil; and the assistance of James Umali, Edson Rodriguez, Hann-Shin Mao, Sophonias Teshome, Sevan Megerian, and Monica Cowan in various stages of these studies.

References

- [1] Margason, R. J., "Fifty Years of Jet in Cross Flow Research," AGARD CP-534, Paper 1, 1993, pp. 1–141.
- [2] Fric, T. F., and Roshko, A., "Vortical Structure in the Wake of a Transverse Jet," *Journal of Fluid Mechanics*, Vol. 279, 1994, pp. 1–47. doi:10.1017/S0022112094003800
- [3] Kelso, R. M., Lim, T. T., and Perry, A. E., "An Experimental Study of Round Jets in Cross-Flow," *Journal of Fluid Mechanics*, Vol. 306, 1996, pp. 111–144. doi:10.1017/S0022112096001255
- [4] Broadwell, J. E., and Breidenthal, R. E., "Structure and Mixing of a Transverse Jet in Incompressible Flow," *Journal of Fluid Mechanics*, Vol. 148, 1984, pp. 405–412. doi:10.1017/S0022112084002408
- [5] Crotelezzi, L., and Karagozian, A. R., "On the Formation of the Counter-Rotating Vortex Pair in Transverse Jets," *Journal of Fluid Mechanics*, Vol. 446, 2001, pp. 347–373.
- [6] Kelso, R., and Smits, A., "Horseshoe Vortex Systems Resulting from the Interaction Between a Laminar Boundary Layer and a Transverse Jet," *Physics of Fluids*, Vol. 7, 1995, pp. 153–158. doi:10.1063/1.868736
- [7] Karagozian, A. R., "Transverse Jets and Their Control," *Progress in Energy and Combustion Science*. doi:10.1016/j.pecs.2010.01.001
- [8] Johari, H., Pacheco-Tougas, M., and Hermanson, J. C., "Penetration and Mixing of Fully Modulated Turbulent Jets in Crossflow," *AIAA Journal*, Vol. 37, No. 7, 1999, pp. 842–850. doi:10.2514/2.7532
- [9] Johari, H., "Scaling of Fully Pulsed Jets in Crossflow," *AIAA Journal*, Vol. 44, No. 11, 2006, p. 2719. doi:10.2514/1.18929
- [10] Narayanan, S., Barooah, P., and Cohen, J. M., "Dynamics and Control of an Isolated Jet in Crossflow," *AIAA Journal*, Vol. 41, No. 12, 2003, pp. 2316–2330. doi:10.2514/2.6847
- [11] Schuller, T., King, J., Majamaki, A., and Karagozian, A. R., "An Experimental Study of Acoustically Controlled Gas Jets in Crossflow," *Bulletin of the American Physical Society*, Vol. 44, 1999, p. 111.
- [12] M'Closkey, R. T., King, J., Crotelezzi, L., and Karagozian, A. R., "The Actively Controlled Jet in Crossflow," *Journal of Fluid Mechanics*, Vol. 452, 2002, pp. 325–335.
- [13] Crotelezzi, L., M'Closkey, R. T., and Karagozian, A. R., "A Framework to Design Controllers for Engineering Applications of Transverse Jets," *Manipulation and Control of Transverse Jets*, edited by A. R. Karagozian, L. Crotelezzi, and A. Soldati, Vol. 439, CISM Courses and Lectures, Springer-Wein, New York, 2003.
- [14] Shapiro, S., King, J., M'Closkey, R. T., and Karagozian, A. R., "Optimization of Controlled Jets in Crossflow," *AIAA Journal*, Vol. 44, No. 6, 2006, pp. 1292–1298. doi:10.2514/1.19457
- [15] Gharib, M., Rambod, E., and Shariff, K., "A Universal Time Scale for Vortex Ring Formation," *Journal of Fluid Mechanics*, Vol. 360, 1998, pp. 121–141. doi:10.1017/S0022112097008410
- [16] Megerian, S., Davitian, J., Alves, L. S. de B., and Karagozian, A. R., "Transverse-Jet Shear-Layer Instabilities. Part 1. Experimental Studies," *Journal of Fluid Mechanics*, Vol. 593, 2007, pp. 93–129.
- [17] Davitian, J., "Exploration and Controlled Excitation of Transverse Jet Shear Layer Instabilities," Ph.D. Thesis, Univ. of California, Los Angeles, Dept. of Mechanical and Aerospace Engineering, Dec. 2008.
- [18] Alves, L. S. de B., Kelly, R. E., and Karagozian, A. R., "Local Stability

- Analysis of an Inviscid Transverse Jet,” *Journal of Fluid Mechanics*, Vol. 581, 2007, pp. 401–418.
doi:10.1017/S0022112007005873
- [19] Alves, L. S. de B., Kelly, R. E., and Karagozian, A. R., “Transverse-Jet Shear-Layer Instabilities. Part 2. Linear Analysis for Large Jet-to-Crossflow Velocity Ratio,” *Journal of Fluid Mechanics*, Vol. 602, 2008, pp. 383–401.
- [20] Monkewitz, P. A., Bechert, D. W., Barsikow, B., and Lehmann, B., “Self-Excited Oscillations and Mixing in a Heated Round Jet,” *Journal of Fluid Mechanics*, Vol. 213, 1990, pp. 611–639.
doi:10.1017/S0022112090002476
- [21] Monkewitz, P. A., Lehmann, B., Barsikow, B., and Bechert, D. W., “The Spreading of Self-Excited Hot Jets by Side Jets,” *Physics of Fluids. A, Fluid Dynamics*, Vol. 1, 1989, p. 446.
doi:10.1063/1.857467
- [22] Sreenivasan, K. R., Raghun, S., and Kyle, D., “Absolute Instability in Variable Density Round Jets,” *Experiments in Fluids*, Vol. 7, No. 5, 1989, pp. 309–317.
- [23] Hallberg, M. P., and Strykowski, P. J., “Open-Loop Control of Fully Nonlinear Self-Excited Oscillations,” *Physics of Fluids*, Vol. 20, 2008, p. 041703.
doi:10.1063/1.2908008
- [24] Strykowski, P. J., and Niccum, D. L., “The Stability of Countercurrent Mixing Layers in Circular Jets,” *Journal of Fluid Mechanics*, Vol. 227, 1991, pp. 309–343.
doi:10.1017/S0022112091000137
- [25] Juniper, M. P., L. K. B. Li., and Nichols, J. W., “Forcing of Self-Excited Round Jet Diffusion Flames,” *Proceedings of the Combustion Institute*, Vol. 32, 2009, pp. 1191–1198.
doi:10.1016/j.proci.2008.05.065
- [26] Canny, J., “A Computational Approach to Edge Detection,” *IEEE Transactions on Pattern Analysis and Machine Intelligence*, Vol. PAMI-8, No. 6, 1986, pp. 679–698.
doi:10.1109/TPAMI.1986.4767851
- [27] Ljung, L., *System Identification: Theory for the User*, 2nd ed., Prentice-Hall, Upper Saddle River, NJ, 1999.
- [28] Pier, B., “Open-Loop Control of Absolutely Unstable Domains,” *Proceedings Of The Royal Society Of London Series A*, Vol. 459, No. 2033, 2003, pp. 1105–1115.
doi:10.1098/rspa.2002.1086
- [29] Huerre, P., and Monkewitz, P. A., “Local and Global Instabilities in Spatially Developing Flows,” *Annual Review of Fluid Mechanics*, Vol. 22, 1990, pp. 473–537.
doi:10.1146/annurev.fl.22.010190.002353
- [30] Reynolds, W. C., Parekh, D. E., Juvet, P. J. D., and Lee, M. J. D., “Bifurcating and Blooming Jets,” *Annual Reviews in Fluid Mechanics*, Vol. 35, 2003, pp. 295–315.
- [31] Bons, J. P., Sondergaard, R., and Rivir, R. B., “The Fluid Dynamics of Lpt Blade Separation Control Using Pulsed Jets,” *Journal of Turbomachinery*, Vol. 124, No. 1, 2002, pp. 77–85.
doi:10.1115/1.1425392
- [32] Ekkad, S. V., Ou, S., and Rivir, R. B., “Effect of Jet Pulsation and Duty Cycle on Film Cooling from a Single Jet on a Leading Edge Model,” *Journal of Turbomachinery*, Vol. 128, No. 3, 2006, pp. 564–571.
doi:10.1115/1.2185122
- [33] Sau, R., and Mahesh, K., “Optimization of Pulsed Jets in Crossflow,” *Journal of Fluid Mechanics*, 2010 (submitted for publication).

N. Chokani
Associate Editor